

Reionization and Structure Formation with ARCADE

A. Kogut¹

Structure formation in the early universe is expected to produce a cosmological background of free-free emission. The Absolute Radiometer for Cosmology, Astrophysics, and Diffuse Emission (ARCADE) will measure the spectrum of the cosmic microwave background at centimeter wavelengths to detect this signature of structure formation. I describe the ARCADE instrument and the cryogenic engineering required to achieve mK accuracy at such long wavelengths.

1 Introduction

In standard cosmological models, the cosmic microwave background (CMB) originates in a hot, dense phase of the early universe. Matter and radiation remain tightly coupled as the universe expands and cools, until the temperature drops sufficiently below the ionization potential of hydrogen at redshift $z \sim 1100$. Structures then emerge through gravitational infall and collapse, until the first collapsed objects ignite in nuclear fusion to re-ionize the intergalactic medium and end the cosmic “dark ages.”

The non-linear collapse of bound structures depends sensitively on poorly known parameters such as the distribution function of rare high-density peaks, the efficiency of competing cooling mechanisms, and the disruptive “feedback” of ionizing radiation from the first objects on successive generations (see, e.g., Tegmark et al. 1997, Gnedin & Ostriker 1997, Haiman & Loeb 1997, Oh 2001). Measurements of the Gunn-Peterson absorption trough in spectra of distant quasars show neutral hydrogen present at $z \approx 6$ (Becker et al. 2001, Djorgovski et al. 2001, Fan et al. 2002). WMAP measurements of correlated temperature-polarization anisotropy, however, show a substantial optical depth to free electrons at much higher redshifts, indicating that reionization occurred within the redshift range $11 < z_r < 30$ (Kogut et al. 2003). The two results are not incompatible – since absorption spectra are sensitive to even small amounts of neutral hydrogen, models with partial ionization $x_e \lesssim 1$ can have enough neutral column density to produce the Gunn-Peterson trough while still providing free electrons to scatter CMB photons and produce large-scale polarization.

Spectral measurements at long wavelengths provide additional information on reionization and structure formation. The ionized intergalactic medium can cool through free-free emission from electron-ion interactions. The distortion to the present-day CMB spectrum is given by

$$\Delta T_{\text{ff}} = T_{\gamma} \frac{Y_{\text{ff}}}{x^2} \quad (1)$$

where T_{γ} is the undistorted photon temperature, x is the dimensionless frequency $h\nu/kT_{\gamma}$, and Y_{ff} is the optical depth to free-free emission (Bartlett & Stebbins 1991). The distortion from a blackbody spectrum varies as ν^{-2} and can be appreciable at sufficiently long wavelengths.

¹Code 685, Goddard Space Flight Center, Greenbelt, MD 20771

Figure 1 illustrates the dependence of cosmological free-free emission on reionization and structure formation. The amplitude of the cosmological free-free signal depends on the column $\int n_e^2$ of ionized gas and thus on the redshift z_r at which the first collapsed objects formed. Using the observed Lyman- α forest, Haiman & Loeb (1997) derive a lower limit $|Y_{\text{ff}}| > 8 \times 10^{-8}$ for the cosmological free-free background originating at redshift $z < 5$, corresponding to a distortion $\Delta T = 0.2$ mK at 2 GHz. Ionized gas at higher redshift will further enhance the signal. Two sources are important. Reionization produces a smoothly-distributed signal at high redshift, while a more clumpy component from halos occurs at intermediate redshift $z \sim 10$. Since $\Delta T \sim n_e^2$, the integrated spectral distortion is strongly weighted to denser regions. Oh (1999) shows that the halo contribution is dominant, with mean distortion $\Delta T \approx 3$ mK at 2 GHz. Measurements at long wavelengths thus probe the thermal history of the universe in the redshift range 10–30 where the bulk of structure formation occurs.

Figure 2 shows current upper limits to CMB spectral distortions. Direct observational limits at long wavelengths are weak: distortions as large as 5% could exist at wavelengths of several centimeters or longer without violating existing observations. Structure formation should produce a cosmological free-free background with amplitude of a few mK at frequencies of a few GHz. Such a signal is well below current observational limits, which only constrain $|Y_{\text{ff}}| < 1.9 \times 10^{-5}$ (Bersanelli et al. 1994).

Long-wavelength measurements of the CMB spectrum are also sensitive to distortions created at earlier epochs ($10^4 < z < 10^7$), described by a Bose-Einstein distribution with dimensionless chemical potential $\mu = 1.4 \Delta E/E$, proportional to the fractional energy release to the CMB (Burigana et al. 1991). The resulting spectrum has a distinctive drop in brightness temperature at centimeter wavelengths (Figure 2). A chemical potential distortion is a primary signature for the decay of relics from GUT and Planck-era physics.

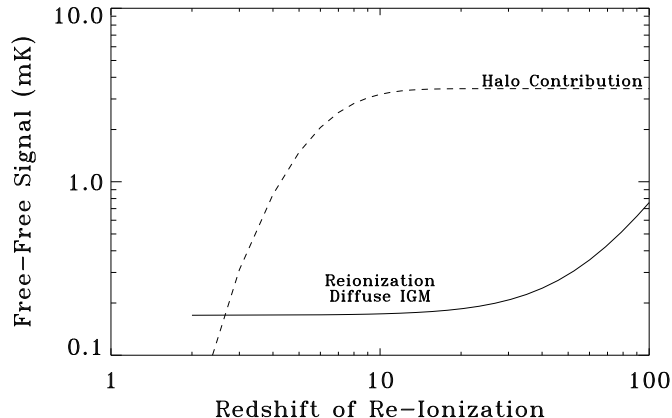


Figure 1: Cosmological free-free signal at 2 GHz as a function of the redshift of reionization. The contribution from clumpy halos at $z \sim 10$ dominates the more smoothly distributed signal from reionization at higher redshifts.

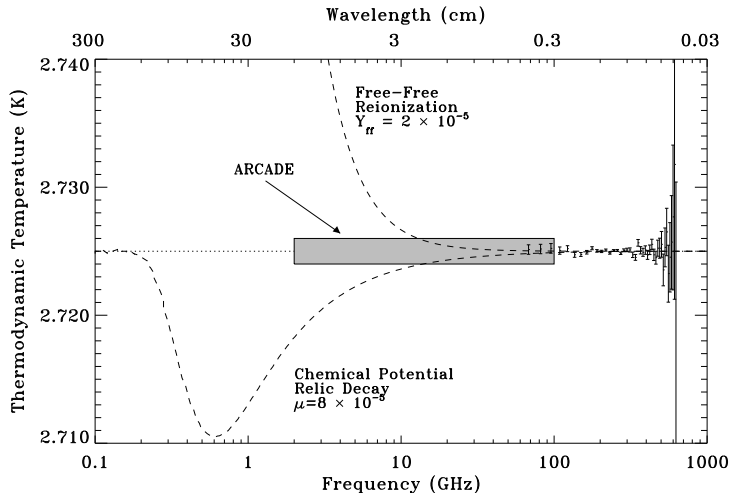


Figure 2: Current 95% confidence upper limits to distorted CMB spectra. The FIRAS data and ARCADE 1 mK error box are also shown; error bars from existing cm-wavelength measurements are larger than the figure height. Free-free emission from reionization and structure formation causes a quadratic increase in temperature at long wavelengths. Energy release at very high redshift ($z > 10^3$) could also create a chemical potential distortion.

2 ARCADE Instrument

The Absolute Radiometer for Cosmology, Astrophysics, and Diffuse Emission (ARCADE) is an instrument designed to detect the cosmological signal from reionization and structure formation through long-wavelength measurements of the CMB spectrum. Figure 3 shows the instrument design. It consists of 6 balloon-borne narrow-band cryogenic radiometers ($\Delta\nu/\nu \sim 10\%$) with central frequencies $\nu = 3.3, 5.5, 8.1, 10.1, 30.3,$ and 89 GHz chosen to cover the gap between full-sky surveys at radio frequencies ($\nu < 2$ GHz) and the FIRAS millimeter and sub-mm measurements. Each radiometer measures the difference in power between a beam-defining antenna (FWHM $\sim 12^\circ$) and a temperature-controlled internal reference load. An independently controlled blackbody target (emissivity $\epsilon > 0.9999$) is located on the aperture plane, and is rotated to cover each antenna in turn, so that each antenna alternately views the sky or a known blackbody.

The ARCADE instrument design greatly reduces all major sources of systematic error in previous long-wavelength spectral measurements. It is a differential instrument with an external blackbody target: instrumental signals thus drop out in the sky–target comparison. It observes above the bulk of the atmosphere, reducing atmospheric emission to below 2 mK. The instrument is fully cryogenic; all major components are independently temperature-controlled to remain at 2.7 K, isothermal with the signal from deep space. Boiloff helium vapor, vented through the aperture plane, forms a barrier between the instrument and the atmosphere; there are no windows or warm optics to correct. All channels observe a common external calibration target, eliminating cross-calibration uncertainties. The experimental precision is limited only by systematic uncertainties associated with operation within the

Earth’s atmosphere and is intended in part to develop technology for the DIMES space mission.

Each radiometer consists of a cryogenic front end with a high electron mobility transistor (HEMT) direct-gain receiver, switched at 1 kHz for gain stability between a wavelength-scaled corrugated conical horn antenna and a temperature-controlled internal load. To reduce insertion loss and the resulting sensitivity to instrument temperature, we switch between the sky horn and internal load using latching ferrite switches whose measured insertion loss is below 0.4 dB. The low insertion loss greatly reduces requirements for thermal monitoring and control of the instrument front end. The back end of each radiometer is split into two frequency sub-channels: a wide-band channel for maximum sensitivity, and a narrow-band channel restricted to protected RF bands. A lockin amplifier in each band demodulates the switched signal to produce an output proportional to the difference in power between the antenna and the internal load. All of the radiometer back ends are housed in a temperature-controlled module mounted to the outside of the dewar.

Each receiver is fed by a corrugated conical horn antenna scaled in wavelength to produce identical beam shape in each frequency channel. To avoid convective instabilities in the helium vapor barrier, the instrument should remain vertical during observations. We reconcile this requirement with the need for sky coverage (and avoiding direct view of the balloon) by mounting the antennas at a 30° angle from the zenith, slicing each antenna at the aperture plane. Quarter-wave chokes surround the resulting elliptical aperture and provide further suppression of side lobes. The cold flares at the dewar rim function as a cold ground shield to block emission from the Earth.

The external target consists of a microwave absorber (Eccosorb CR-112, an iron-loaded epoxy) cast with grooves in the front surface to reduce reflections. The Eccosorb is mounted on a series of thermally conductive plates with conductance G_1 separated by

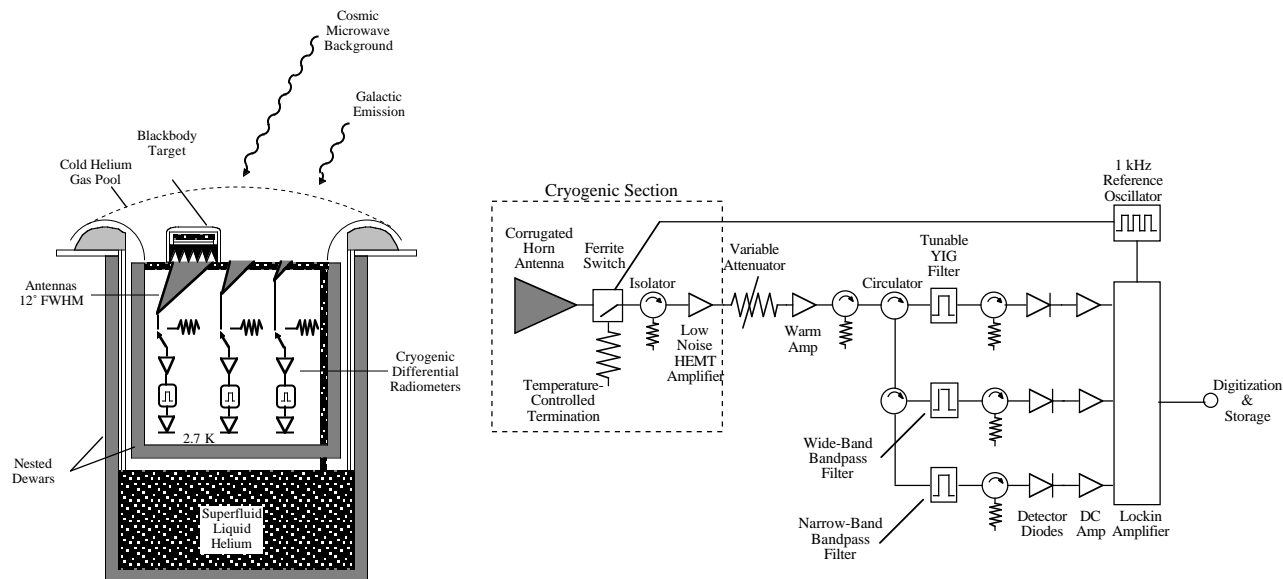


Figure 3: (Left) Schematic drawing of ARCADE instrument. (Right) Block diagram of ARCADE radiometers.

thermal insulators of conductance G_2 . Thermal control is achieved by heating the outermost buffer plate, which is in weak thermal contact with a superfluid helium reservoir. Radial thermal gradients at each stage are reduced by the ratio G_2/G_1 between the buffer plates. Fiberglass and copper achieve a ratio $G_2/G_1 < 10^{-3}$; a two-stage design should achieve net thermal gradients well below 1 mK, verified both in the lab and in flight using embedded ruthenium oxide thermistors. We calibrate the thermistors *in situ* by immersing the target in a LHe bath, then recording data through the flight thermal readout system as the pressure above the bath is varied. This calibrates out residual (nW) self-heating in each thermometer while providing accurate cross-calibration between thermometers to limit thermal gradients in flight. The readout system has demonstrated in-flight white noise below 0.2 mK Hz^{-1/2} (Fixsen et al. 2002). We have measured the target power reflection coefficient with the target in place over the flight antennas. The resulting upper limits $R < -35$ dB exceed the -30 dB design requirement.

ARCADE’s observing strategy is straightforward. Independent thermal control in each channel adjusts the internal load temperatures to null the radiometer outputs when the antennas view the sky. We then adjust the external target temperature to exactly null the sky signal in the longest-wavelength channel. With all temperatures held constant, the target will then move to cover the short-wavelength antennas. If the sky were a perfect blackbody, all shorter-wavelength channels would also show a null between the sky and target. ARCADE will thus measure small spectral shifts about a precise blackbody, greatly reducing dependence on instrument calibration and stability. By comparing each channel to the *same* external target, uncertainties in the target temperature cancel so that deviations from a blackbody spectral *shape* may be determined much more precisely than the absolute temperature. The ARCADE nulling scheme allows more than an order of magnitude improvement over previous cm-wavelength measurements, and is directly analogous to the nulling used to achieve 50 parts-per-million accuracy by the FIRAS experiment (Mather et al. 1999).

3 Stupid Dewar Tricks

Figure 4 shows the gondola design for the 2001 flight. It consists of a 3.7 m frame with the dewar on one end. Batteries and flight electronics serve as counterweights on the other end, allowing the suspension to be located well away from the dewar.

The ARCADE design has a fully cryogenic clear aperture operating without windows or any view to warm components. Achieving this in practice requires some innovative cryogenic engineering. Normally, one might isolate the instrument from ambient (250 K) conditions by putting the cryogenic components toward the bottom of the dewar. But this would entail some view of the dewar wall, which necessarily has a large temperature drop. In order to eliminate any emission from the dewar walls, the ARCADE aperture plane is located at the *mouth* of an open bucket dewar, using a second (internal) dewar to reduce radial heat transport between the 2.7 K optics and the 250K exterior wall some 20 cm away. To keep the aperture cold, ARCADE uses fountain-effect pumps to move superfluid LHe from storage in the bottom of the dewar to reservoirs located in the aperture plane and ex-

ternal calibration target. Boiloff gas passes through pinholes in the aperture plane, providing additional cooling through the enthalpy of the gas.

ARCADE operates at altitudes above 33 km. An ascent lid covers the aperture during launch, then opens to allow observations of the sky. Once the lid is open, we prevent condensation of atmospheric nitrogen onto the cold optics using boiloff He gas. Helium gas at ambient pressure of 3 Torr is denser than atmospheric nitrogen provided the helium remains colder than 20 K. Stainless steel flares, also cooled by boiloff gas, surround the cryogenic aperture to trap a pool of cold He gas over the optics. Resistive heaters in the LHe reservoir provide control over the He gas flow, which can be increased to maintain cold enough temperatures above the aperture plane.

We have successfully flown a 2-channel prototype to validate the open-aperture cryogenic design, demonstrating the ability to control the radiometer front end and cold optics at 2.7 K. Figure 5 shows an image of the aperture plane taken during the November 2001 flight. More than 30 minutes after opening the lid, only a few mm of condensation has formed. Thermal data from the same flight are consistent with slow ice accumulation of 0.1 g/s. Nitrogen condensation did *not* begin immediately after the ascent lid opened, but was apparently triggered 5 minutes later by turbulent mixing above the aperture plane. Despite the slow buildup, we were able to obtain over 30 minutes of good data on the sky, sufficient to measure the CMB spectrum. Since the instrument is nearly isothermal with the CMB and nitrogen ice is nearly transparent to microwaves, minor condensation on the flight optics will not cause significant effects. Following the November 2001 flight, we have modified the aperture plane to decrease turbulent mixing and further reduce nitrogen condensation. A kW heater on the aperture plane now provides the ability to remove accumulated ice several times per flight.

Mechanical failure of the external target position control limited science returns from

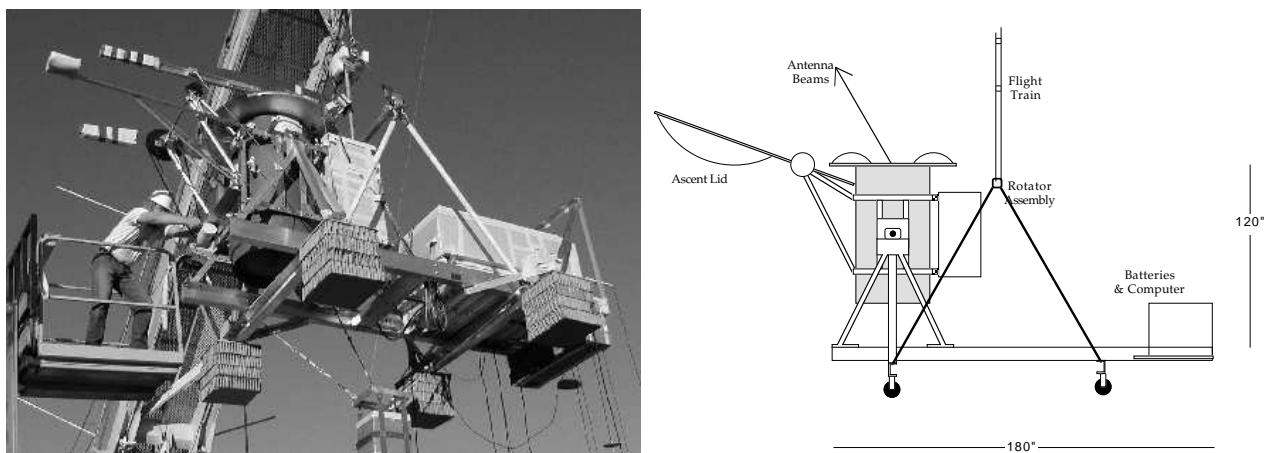


Figure 4: (left) Payload in 2001 configuration with 2-channel prototype instrument. (right) Gondola schematic for 2001 flight. The dewar is counter-balanced by the batteries and flight electronics.

the first flight. A second flight is scheduled for summer 2003 to test the modified aperture plane, including the de-icing heater. This second flight will compare the CMB temperature between 10 and 30 GHz to accuracy of a few mK. A larger version using all 6 channels is under construction and is expected to fly before 2005.

4 Error Budget

ARCADE will not be limited by raw sensitivity. HEMT amplifiers cooled to 2.7 K easily achieve *rms* noise $\sim 1 \text{ mK Hz}^{-1/2}$: a few seconds integration provides all the sensitivity required. We verify that the 1/f knee is below the corresponding frequency of 0.03 Hz. Table 1 summarizes the ARCADE error budget. ARCADE is designed to reduce, eliminate, or control the major sources of systematic uncertainty which have limited previous spectral measurements at centimeter wavelengths. The ARCADE spectra are derived from comparison of the sky to the external blackbody target in multiple frequency channels, and are thus sensitive only to the *difference* of systematic effects from channel to channel.

The largest systematic uncertainties arise from emission of warm objects outside the dewar (the flight train and Earth). We estimate a worst-case signal from the flight train using the gondola geometry and measured beam patterns. The rotator, flight train, and suspension cables will be hidden behind reflectors to redirect the beam to blank areas of the sky. The signal from the reflectors is dominated by their emission and by stray glints to the ground. The largest signals are from the atmosphere, balloon, and flight train. The flight train is situated at nearly the same relative geometry with respect to all antennas, partially cancelling this signal in the differential sky spectra. We will further reduce the uncertainty by using tip scans and azimuthal rotation to modulate the signal from the flight

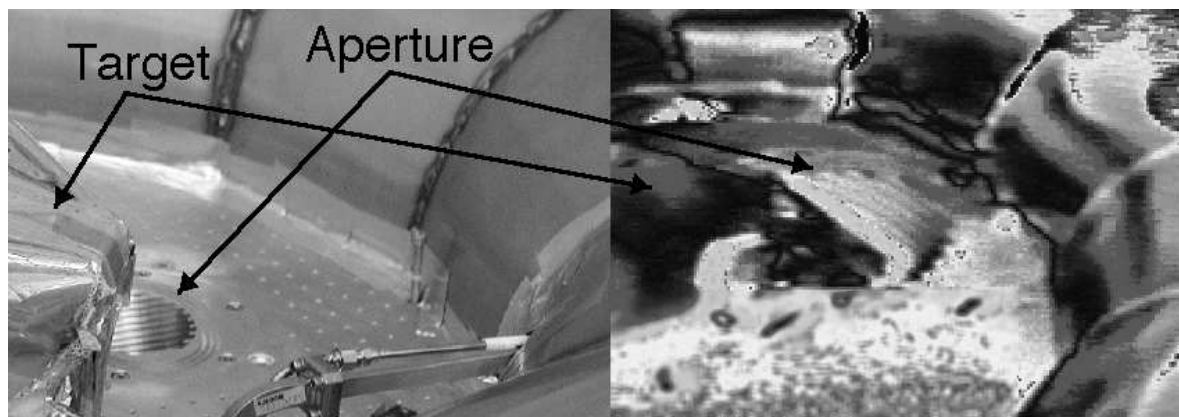


Figure 5: Aperture plane with target and antenna aperture. (left) 30 GHz aperture during ground testing. The target is visible in the left foreground; the cold flares are in the background. (right) Video still taken in flight, 30 minutes after opening ascent lid. The corrugations of the 10 GHz aperture are visible behind the target in the foreground – nitrogen condensation is not a major problem.

Table 1: ARCADE Error Budget

Source	Measurement Technique	Amplitude and Uncertainty (mK)		
		3 GHz	10 GHz	90 GHz
Earth	Beam, Tip Scan	1 ± 0.5	0.3 ± 0.2	0.3 ± 0.2
Flare Emission	Beam, Thermistors	1.5 ± 0.5	0.5 ± 0.2	0.5 ± 0.2
Flight Train	Tip Scan, Screen	3.6 ± 1.2	3.6 ± 1.2	3.6 ± 1.2
Balloon	Beam, Tip Scan	0.2 ± 0.1	1.7 ± 0.5	3.6 ± 1.8
Target Gradients	Thermistors	1.0 ± 0.5	0.3 ± 0.2	0.3 ± 0.2
Target Drifts	Thermistors	0.2 ± 0.2	0.2 ± 0.2	0.2 ± 0.2
Atmosphere	Altitude, Tip Scan	1.4 ± 0.05	1.6 ± 0.06	9.8 ± 0.4
Target Reflection	Lab	<0.1	<0.1	<0.1
Calibration	Target Temperature	<0.1	<0.1	<0.1
Noise	Lab, Binning	<0.1	<0.1	<0.1
Quadrature Uncertainty		± 1.5	± 1.4	± 2.2

train. Ground screens may provide still further reduction. The combination of differential measurement, tip scans, rotational modulation, and screens will reduce the uncertainty in flight train emission or reflection by a factor of 2–3. A similar exercise provides an in-flight estimate for reflection from the balloon; since the balloon is nearly transparent below 10 GHz it contributes mainly to the signal in the high-frequency channels.

The cold flares at the dewar rim function as a cold ground shield to block emission from the Earth: emission from the Earth must diffract over the curved flares before reaching the antenna side lobes. The antenna gain at the flare edges varies from -45 dB in the forward direction to -75 dB in the far back lobes. Diffraction over the flares provides additional attenuation. We have measured the far-field beam pattern of the assembled payload (including the flares) over 4π sr. Based on the measured back-lobe response, the Earth should contribute less than 1 mK to any channel. Both the flight train and Earth signals vary as the gondola is tipped. We will use the in-flight tip scans to verify the predicted signals.

Atmospheric emission at 35 km altitude contributes approximately 1 mK at 10 GHz. Below 10 GHz the spectrum is flat; even if the absolute amplitude were unknown the spectral curvature would contribute less than 0.2 mK differential signal between channels. To first order, we will model this differential signal using models of atmospheric transmission (Liebe 1981; Danese & Partridge 1989). We will confirm the model by correlating the sky-target difference spectra with airmass as the balloon changes altitude during flight. Tip scans in which the dewar tilts 15° in either direction from the zenith provide a second cross-check on atmospheric emission.

Bartlett, J.G., and Stebbins, A., 1991, ApJ, 371, 8

Becker, R. H., et al. 2001, AJ, 122, 2850

Bennett, C. L., et al. 2003, ApJ, in press

Bersanelli, M., et al. 1994, ApJ, 424, 517

Danese, L., and Partridge, R.B. 1989, ApJ, 342, 604
Djorgovski, S.G., et al. 2001, ApJ, 560, L5
Fan, X., et al. 2002, AJ, 123, 1247
Fixsen, D.J., Mirel, P., Kogut, A., and Seiffert, M., 2002, Rev. Sci. Inst, 73, 3659
Gnedin, N.Y., and Ostriker, J.P. 1997, ApJ, 486, 581
Haiman, Z., and Loeb, A. 1997, ApJ, 483, 21
Kogut, A., et al. 2003, ApJ, in press
Liddle, A.R. and Lyth, D.H. 1995, MNRAS, 273, 1177
Liebe, H.J. 1981, Radio Science, 16, 1183
Mather, J., et al., 1999, ApJ, 512, 511
Oh, S. P. 1999, ApJ, 527, 16
Oh, S. P. 2001, ApJ, 553, 499
Tegmark, M., et al. 1997, ApJ, 474, 1